Recapturing lost evanescent power by tuning end face total internal reflection capable tunneling modes at a roughened fiber end face

Jianjun Ma,[1,*] Yasser Chiniforooshan,[1] Jiahua Chen,[1] Wojtek J. Bock,[1] Wenhui Hao,[2] and Zhi Yuan Wang[2]

[1]*Centre de recherche en photonique, Département d'informatique et d'ingénierie, Université du Québec en Outaouais, P. O. Box 1250, Hull Station, Gatineau, Québec J8X 3X7, Canada*

[2]*Department of Chemistry, Carleton University, 1125 Colonel By Drive, Ottawa, Ontario, K1S 5B6, Canada*

**Corresponding author: ma.jianjun@uqo.ca*

Received July 7, 2011; accepted August 13, 2011;
posted August 19, 2011 (Doc. ID 150684); published September 9, 2011

We reveal that the overall evanescent wave (EW) power captured by an unclad multimode fiber employed in a sensing configuration is determined by the tunneling modes, not the guided modes. While enormous in strength, most of this power is inaccessible using traditional EW power enhancers. However, we found that by roughening the fiber end face, this supposedly lost power can be recaptured and thus can boost the detectable power level significantly. Intensive mode mixing events across various mode categories are proposed to interpret the observed phenomenon.

OCIS codes: 060.2270, 060.2370, 300.6280.

When examining various evanescent wave (EW) fiber-optic sensors, we will almost certainly find that each of them has some kind of EW power enhancer. Among the best known are fiber tapers [1], sol–gel overlays [2], long sensing fibers, U-shaped sensing segments, and single-mode fibers with a greater EW field penetration depth. While different in appearance, these enhancers share two common drawbacks. First, all must be immersed in a sample in order to work. An obvious problem here is that despite their fragility, the unclad enhancer segments must be left unprotected to access the sample, posing a particular challenge for a long and/or thin sensing fiber. Negative effects from contact between sol–gel and the sample such as diffusion response time have been reported as well [2]. Second, they suffer from a huge loss of the EW power. Examples in Fig. 1 show that after being excited, the sensing segment receives initial EW power components $I_{EW0}(+)$ and $I_{EW0}(-)$, traveling in opposite directions and obeying $I_{EW0}(+) \equiv I_{EW0}(-)$. The total power, defined as I_{Stotl}, is

$$I_{Stotl} = I_{EW0}(+) + I_{EW0}(-) = 2 \times I_{EW0}(\pm). \tag{1}$$

However, the received power I_R benefits only partially from $I_{EW0}(+)$ and not from $I_{EW0}(-)$ at all. More than half the total power I_{Stotl} is lost.

In this Letter, we investigate the power I_{Stotl} captured by an unclad segment by considering the mode populations and their EW field penetration depths. Then a highly efficient enhancer, the roughened fiber end face, is demonstrated to recapture the lost power component $I_{EW0}(-)$.

For an EW-based multimode (MM) fiber sensor, both guided [1] and tunneling modes [3,4], with their respective populations of N_g and N_t, will participate in collecting the EW power. Mode populations N_g and N_t are considered to be roughly equal (Chap. 24 of [4]) via normalized frequency V [5]:

$$N_t \approx N_g = V^2/2 = \pi^2 d^2 (n_{co}^2 - n_{cl}^2)/2\lambda^2, \tag{2}$$

where n_{co} and n_{cl} are the refractive indices (RIs) of the core and the cladding while d is the core diameter.

Figure 2(a) illustrates an MM fiber with one of its ends decladded and immersed into the liquid sample. The RIs of the core, cladding, and liquid are $n_{co} = 1.46$, $n_{cl} = 1.41$ and $n_{lq} = 1.33$, respectively. Using superscript cl and lq to indicate the corresponding cladding types, the calculation from Eq. (2) shows

$${}^{cl}N_{g,t} \approx 40\% {}^{lq}N_{g,t}. \tag{3}$$

Equation (3), depicted by two histogram bars in Fig. 2(b), suggests that 60% of the modes permitted by the liquid-clad segment is blocked by the clad fiber, whose population is defined as the sum of ${}^{lq}\Delta N_g$ and ${}^{lq}\Delta N_t$:

$${}^{lq}\Delta N_g = 1.5 {}^{cl}N_g \quad \text{and} \quad {}^{lq}\Delta N_t = 1.5 {}^{cl}N_t. \tag{4}$$

The EW field penetration depths of the guided and tunneling modes, defined by δ_g and δ_t, respectively, obey

$$\begin{aligned} &{}^{lq}\delta_{g\_i} > {}^{cl}\delta_{g\_j} \quad \text{and} \quad {}^{lq}\delta_{t\_k} > {}^{cl}\delta_{t\_l}, \qquad i \in {}^{lq}\Delta N_g, \\ &j \in {}^{cl}N_g, \qquad k \in {}^{lq}\Delta N_t, \qquad l \in {}^{cl}N_t. \end{aligned} \tag{5}$$

Equation (5) is valid since any mode within $i \in {}^{lq}\Delta N_g$ or $k \in {}^{lq}\Delta N_t$ has a higher mode-order than modes within $j \in {}^{cl}N_g$ or $l \in {}^{cl}N_t$ and thus a greater penetration depth. Furthermore, ${}^{lq}\delta_{g\_i} \gg {}^{cl}\delta_{g\_j}$ is valid for a large number of low-order modes from ${}^{cl}N_g$ since these low-order modes are well confined within the core and thus are considered

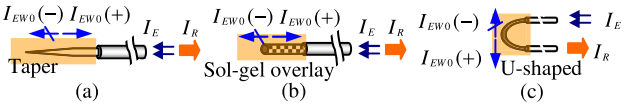

Fig. 1. (Color online) Three traditional fiber-optic EW platforms that fail to access $I_{EW}(-)$: (a) fiber taper, (b) sol–gel overlay, (c) U-shaped segment. I_E is the excitation power and I_R is the received EW power after exiting from the clad fiber.

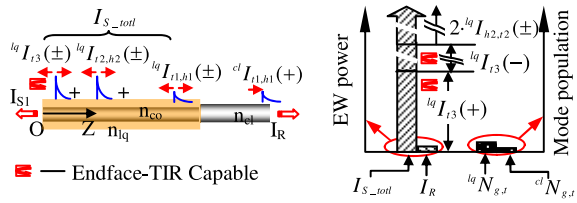

Fig. 2. (Color online) Dependence of EW power collection on the mode groups. (a) Clad fiber with an unclad segment showing permitted mode groups and penetration depths. (b) Histogram showing mode populations and EW power for associated segments.

not to participate in the EW power collection. This fact, together with Eqs. (4) and (5), points to an enormous loss of the EW power in the clad fiber. The discussions so far suggest

$$I_R \ll I_{EW0}(+), \tag{6}$$

$$I_{EW0}(\pm) = {}^{\mathrm{lq}}I_{h,t}(\pm), \tag{7}$$

$$I_{\mathrm{Stotl}} = 2 \times {}^{\mathrm{lq}}I_{h,t}(\pm). \tag{8}$$

In Fig. 2(a), $I_{EW0}(-)$ will not completely exit at $Z = 0$. Instead, the total internal reflection (TIR) of a group of tunneling rays at this end face (end face TIR) [3] leads to a weaker exit power, defined as I_{S1}:

$$I_{S1} < I_{EW0}(-) = {}^{\mathrm{lq}}I_{h,t}(-). \tag{9}$$

Also in Fig. 2(a), the modes contributing to I_{Stotl} are divided into the high-order mode groups $h1$, $h2$ and the tunneling mode groups $t1$, $t2$, and $t3$. The groups $h1$ and $t1$ are permitted by all segments and obey ${}^{\mathrm{lq}}N_{h1,t1} = {}^{\mathrm{cl}}N_{h1,t1}$. The groups $h2$, $t2$, and $t3$ are only permitted by the air- and liquid-clad segments. From Eqs. (4) and (5),

$$\begin{aligned} &{}^{\mathrm{lq}}N_{h2,t2,t3} = {}^{\mathrm{lq}}\Delta N_g + {}^{\mathrm{lq}}\Delta N_t >> {}^{\mathrm{cl}}N_{h1,t1}, \quad \text{and} \\ &{}^{\mathrm{lq}}\delta_{h2\_i} > {}^{\mathrm{cl}}\delta_{h1\_j}, \qquad {}^{\mathrm{lq}}\delta_{(t2,t3)\_k} > {}^{\mathrm{cl}}\delta_{t1\_l}, \qquad i \in {}^{\mathrm{lq}}N_{h2}, \\ &j \in {}^{\mathrm{cl}}N_{h1}, \qquad k \in {}^{\mathrm{lq}}N_{t2,t3}, \qquad l \in {}^{\mathrm{cl}}N_{t1}. \end{aligned} \tag{10}$$

The $t3$ group represents the modes that are end face TIR capable, which is specifically indicated by the small inset in Fig. 2. Equation (10) implies

$$\begin{aligned} &I_R = {}^{\mathrm{cl}}I_{h1,t1}(+) \ll \sum_k {}^{\mathrm{lq}}I_k(-), \\ &k = h2, t2, t3. \end{aligned} \tag{11}$$

Equation (7) can be written in the form

$${}^{\mathrm{lq}}I_i(+) \equiv {}^{\mathrm{lq}}I_i(-), \qquad i = h1, t1, h2, t2, t3, \tag{12}$$

$${}^{\mathrm{lq}}I_j(\pm) \equiv {}^{\mathrm{cl}}I_j(+), \qquad j = h1, t1. \tag{13}$$

The overall EW power of the unclad segment I_{Stotl} is

$$\begin{aligned} &I_{\mathrm{Stotl}} = 2 \times \sum_i {}^{\mathrm{lq}}I_i(+), \\ &i = h1, t1, h2, t2, t3. \end{aligned} \tag{14}$$

From Eqs. (9) and (14), the power level I_{S1} is

$$I_{S1} = \sum_k {}^{\mathrm{lq}}I_k(-) < 50\% I_{\mathrm{Stotl}}, \qquad k = h1, t1, h2, t2, \tag{15}$$

where the $t3$ group is excluded due to the end face TIR effect. Equations (11) and (14) yield

$$I_R \ll 50\% I_{\mathrm{Stotl}}. \tag{16}$$

For the $t3$ mode group, our study shows [3]

$$I_R < 9\% {}^{\mathrm{lq}}I_{t3}(+), \tag{17}$$

where ${}^{\mathrm{lq}}I_{t3}$ is the power from tunneling mode group $t3$ alone. Since the $t3$ mode group contains only part of ${}^{\mathrm{lq}}N_t$, Eqs. (11) and (17) imply that in comparison to the $h2 + t2 + t3$ group, the $h1 + t1$ group will capture a negligible level of EW power. Moreover, from Eqs. (3)–(5) and excluding the $t3$ group, we can still write

$$I_R \ll I_{S1} \approx {}^{\mathrm{lq}}I_{h2,t2}. \tag{18}$$

Equations (14), (17), and (18) are illustrated by two sets of histogram bars in Fig. 2(b). To ease the comparison, first the bar of I_R is plotted at the same height as ${}^{\mathrm{cl}}N_{g,t}$. Bar ${}^{\mathrm{lq}}I_{\mathrm{Stotl}}$ is then constructed by superposing bars of each component in Eq. (14). Among them, bar ${}^{\mathrm{lq}}I_{t3}(-)$ is added on top of ${}^{\mathrm{lq}}I_{t3}(+)$ according to Eq. (12) and the conservative estimate $I_R = 9\% {}^{\mathrm{lq}}I_{t3}(+)$ in Eq. (17). The contributions of ${}^{\mathrm{lq}}I_{t3}(-)$ and ${}^{\mathrm{lq}}I_{h2,t2}(\pm)$ are plotted as broken bars with an upward arrow to imply the huge scale of ${}^{\mathrm{lq}}I_{\mathrm{Stotl}}$. Far exceeding I_R, bar ${}^{\mathrm{lq}}I_{\mathrm{Stotl}}$ reveals that it is the EW field penetration depth, not the mode population, that dominates the EW power collection capability of the sensing segment. If we recall that the purpose of an EW power enhancer is to access the enormous level of the blocked I_{Stotl}, it is clear that an enhancer solely dependent on a longer fiber for sensing, whose I_R is illustrated in Fig. 2(b), will have the lowest efficiency. Moreover, Eqs. (2) and (4) suggest

$${}^{\mathrm{lq}}\Delta N_t > {}^{\mathrm{lq}}\Delta N_{h2}. \tag{19}$$

Since all tunneling modes operate just below cutoff [4] and most $h2$ modes operate far from cutoff with only a few of them near cutoff, it is valid to write

$${}^{\mathrm{lq}}\delta_{t\_i} > {}^{\mathrm{lq}}\delta_{h2\_j}, \qquad i \in {}^{\mathrm{lq}}\Delta N_t, \qquad j \in {}^{\mathrm{lq}}\Delta N_{h2}. \tag{20}$$

Applying Eqs. (19) and (20) to Eq. (14) and ignoring the $h1 + t1$ group, the level of I_{Stotl} is obviously determined by the tunneling modes rather than the guided modes. Further, the enhancer mechanisms in Fig. 1 can partially access ${}^{\mathrm{lq}}I_{t2,h2}(+)$. The components ${}^{\mathrm{lq}}I_{t2,h2}(-)$ and ${}^{\mathrm{lq}}I_{t3}(\pm)$

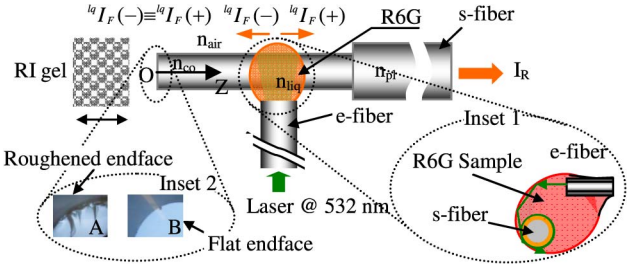

Fig. 3. (Color online) Fiber-optic EW sensing platform to demonstrate the enhancer based on a roughened end face. A liquid droplet of R6G water solution represents the fluorescence-capable sample.

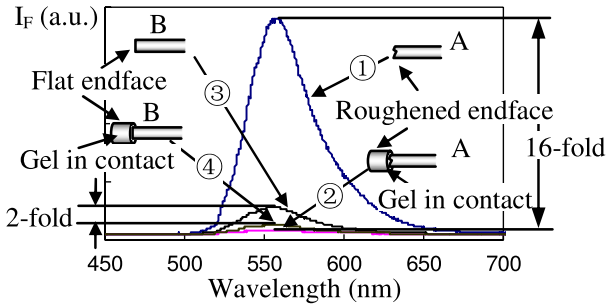

Fig. 4. (Color online) Experimental results for the roughened fiber end face A and flat end face B.

are completely lost even if we attach a mirror at the end face since its mechanism cannot overcome the inhibition of the $h2 + t2 + t3$ group in the clad fiber.

We now propose a simple enhancer—a roughened fiber end face—to significantly increase I_R by feeding a fraction of the normally inaccessible EW power ${}^{lq}I_{h2,t2,t3}(-)$ into the modes permitted by the clad fiber. As shown in Fig. 3, the platform includes two identical fibers with a core diameter of 400 μm and RIs as above. They are perpendicular to each other with one for sensing (s-fiber) and one to deliver the excitation (e-fiber) light. A rhodamine 6G (R6G) water solution is used as the fluorescence-capable sample to surround approximately 2 mm of the unclad segment. Inset 1 illustrates the optimum offset among the s-fiber, e-fiber, and R6G droplet, achieved by shaping the droplet via surface tension until the maximum fluorescent EW power I_R is observed [6]. Two fibers with different types of end face roughness were prepared, as shown in Inset 2. Under a microscope, the end face of fiber A, after being treated by a diamond-tipped fiber scribe, shows a roughened end face with many chipped areas randomly distributed at its outmost edge. The end face of fiber B is flat after being treated by a standard polishing process. The RI matching gel with an RI of 1.462 was used to eliminate the end face TIR effect when needed. From Eqs. (7) and (14), we have

$$ {}^{lq}I_F(\pm) = \sum_i {}^{lq}I_i(+) = 50\% I_{Stotl}, \qquad i = h1, t1, h2, t2, t3. \tag{21}$$

As discussed before, normally ${}^{lq}I_F(-)$ or ${}^{lq}I_{h2,t2,t3}(-)$ is lost to the clad fiber. This is valid for the flat end face of the unclad segment. For the roughened end face of fiber A, we notice three critical facts. First, the chipped edge (Inset 2 of Fig. 3) is also occupied by the major portion of the mode fields of the $h2 + t2 + t3$ groups. Second, the most sensitive to these chipped areas is the $t3$ group due to its end face TIR capability. Third, as a subset of the vast number of ${}^{lq}\Delta N_{g,t}\tilde{1} \times 10^6$ calculated from Eq. (4), the population ${}^{lq}N_{t3}$ is also large. These facts together suggest that an intense mode tuning event will be triggered by the chipped edge upon reflection, resulting in a portion of power being transferred from the $t3$ group to the $h1$ or $t1$ group, which can be added to I_R. In contrast, the flat end face of fiber B lacks the mode-mixing mechanism and thus eliminates the influence of the $h2 + t2 + t3$ group on I_R. The experimental results in Fig. 4 indicate that curves 2 and 4, described by Eq. (11), remain nearly horizontal after the total elimination of the end face TIR with RI gel. However, curve 1 shows an enormous 16-fold increase of I_R over curve 2 when the roughened end face is exposed to air, proving that the roughened end face triggered the mode tuning. In other words, over 94% of I_R is generated by this end face tuning alone. Yet, for the flat end face also given in Fig. 4, a mere twofold increase of I_R from curve 4 to curve 3 is observed, confirming the analysis for the flat end face. Curves 2 and 4 prove again that, due to the lack of contribution from ${}^{lq}I_{h2,t2,t3}(\pm)$, the enhancer depending solely on a longer fiber is extremely inefficient.

In conclusion, dominated by the tunneling modes, the EW power ${}^{lq}I_{Stotl}$ given in Fig. 2(b) is so strong that in many applications, the level of I_R from a short sampling section (2 mm long in our case), might be sufficient for detection. Moreover, traditional enhancers benefit from only a small amount of ${}^{lq}I_{Stotl}$ at the cost of introducing difficult-to-implement techniques and problematic enhancer–sample interactions. In contrast, this enhancer based on a roughened end face is not only remarkably simple and efficient but also eliminates any need for change in the rest of the system. All that is needed is to deliberately lower the quality of the fiber end face—an easy procedure involving only a tiny 400 μm diameter surface area. Finally, this enhancer avoids issues stemming from the enhancer–sample contact summarized before since it has no contact whatsoever with the sample.

The authors gratefully acknowledge support for this work from the Natural Sciences and Engineering Research Council of Canada, from the Canada Research Chairs Program, and from the Ministère de Développement économique, Innovation et Exportation du Québec.

References

1. J. P. Golden, G. P. Anderson, S. Y. Rabbany, and F. S. Ligler, IEEE Trans. Biomed. Eng. **41**, 585 (1994).
2. B. D. MacCraith, C. McDonagh, A. K. McEvoy, T. Butler, G. O'Keeffe, and V. Murphy, J. Sol-Gel Sci. Technol. **8**, 1053 (1997).
3. J. Ma, W. J. Bock, and A. Cusano, Opt. Express **17**, 7630 (2009).
4. A. W. Snyder and J. D. Love, *Optical Waveguide Theory* (Chapman & Hall, 1983).
5. D. Gloge, Appl. Opt. **10**, 2252 (1971).
6. J. Ma and W. J. Bock, Opt. Lett. **32**, 8 (2007).